ACS OMEGA

http://pubs.acs.org/journal/acsodf

Article

Tailored Synthesis of Iron Oxide Nanocrystals for Formation of Cuboid Mesocrystals

Zeliha Soran-Erdem, Vijay Kumar Sharma, Pedro Ludwig Hernandez-Martinez, and Hilmi Volkan Demir*

Cite This: *ACS Omega* 2021, 6, 20351−20360

Read Online

ACCESS | Metrics & More | Article Recommendations | Supporting Information

ABSTRACT: In this work, we systematically studied the shape- and size-controlled monodisperse synthesis of iron oxide nanocrystals (IONCs) for their use as building blocks in the formation of mesocrystals. For this aim, on understanding the influence of the oleic acid concentration, iron-oleate concentration, and heating rate on the synthesis of robust and reproducible IONCs with desired sizes and shapes, we synthesized highly monodisperse ∼11 nm sized nanocubes and nanospheres. Magnetic measurements of both cubic and spherical IONCs revealed the presence of mixed paramagnetic and superparamagnetic phases in these nanocrystals. Moreover, we observed that the magnetic moments of the nanocubes are more substantial compared to their spherical counterparts. We then demonstrated a simple magnetic-field-assisted assembly of nanocubes into three-dimensional (3D) cuboid mesocrystals while nanospheres did not form any mesocrystals. These findings indicate that small cubic nanocrystals hold great promise as potential building blocks of 3D magnetic hierarchical structures with their superior magnetic properties and mesocrystal assembly capability, which may have high relevance in various fields ranging from high-density data storage to biomedical applications.

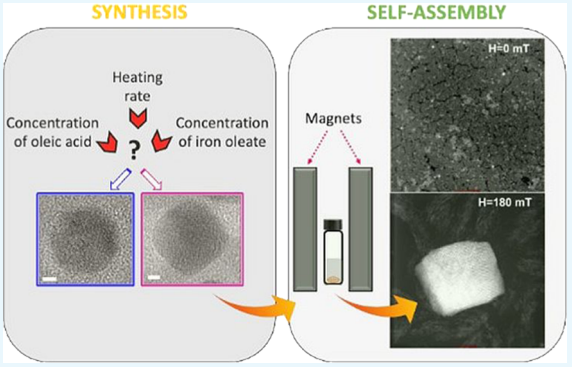

INTRODUCTION

Self-assembly of nanocrystal order over a microscopic size regime is one of the hot research topics nowadays. Mesocrystals are crystallographically oriented nanocrystals showing different physical and chemical features from their corresponding bulk materials[1] and have found applications in photocatalysis, solar energy, energy storage, and optoelectronics.[1−3] While magnetite bulk single crystals have a ferrimagnetic nature, mesocrystals of superparamagnetic (SPM) nanocrystals smaller than 30 nm retain their superparamagnetic properties and even have tens or hundreds of micrometers.[4] These well-ordered superlattices possess much higher magnetization than that of individual nanocrystals.

Self-assembly of magnetic nanocrystals depends on a range of parameters such as initial particle concentration, nanocrystal composition, surrounding ligand shell, interparticle interactions, and external magnetic interactions.[5,6] Additionally, the morphology of the nanocrystals and their narrow size distribution are other influencing parameters in the controlled self-assembly of nanocrystals.[7] Recently, cubic iron oxide nanocrystals (IONCs) have been studied for magnetic-field-induced assembly into one-dimensional (1D) chains, two-dimensional (2D) monolayer sheets, and three-dimensional (3D) ordered arrays and mesocrystals.[8−13] In one of these studies, Ahniyaz et al.[10] observed mesocrystals of maghemite nanocubes when the magnetic field was applied during the entire duration of the drying-mediated assembly process. On the contrary, there is also a report showing the formation of mesocrystals in both the absence and the presence of a magnetic field.[8] In this study, researchers claim that the specific ordering of nanoparticles induced during the assembly process is controlled by the competition of two types of anisotropic interactions: the face-to-face alignment is caused by the particle shape, while the alignment along the magnetic field lines is driven by the orientation of the magnetic moment of the nanoparticles. In light of these different studies, it is understood that mesocrystal formation is a complex process, and the mechanism behind the mesocrystals using magnetic IONCs is not fully understood.

IONCs have a rich phase diagram with various oxidation states, making it more complicated to control the synthesis of IONCs with uniform size and shape.[14] Moreover, the intrinsic agglomerating feature of magnetic nanocrystals is a drawback for the monodisperse synthesis of IONCs.[15] To date, various mechanochemical techniques (mechanical milling, pyrolysis,

Received: May 3, 2021
Accepted: June 25, 2021
Published: August 2, 2021

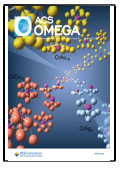

https://doi.org/10.1021/acsomega.1c02322
ACS Omega 2021, 6, 20351−20360

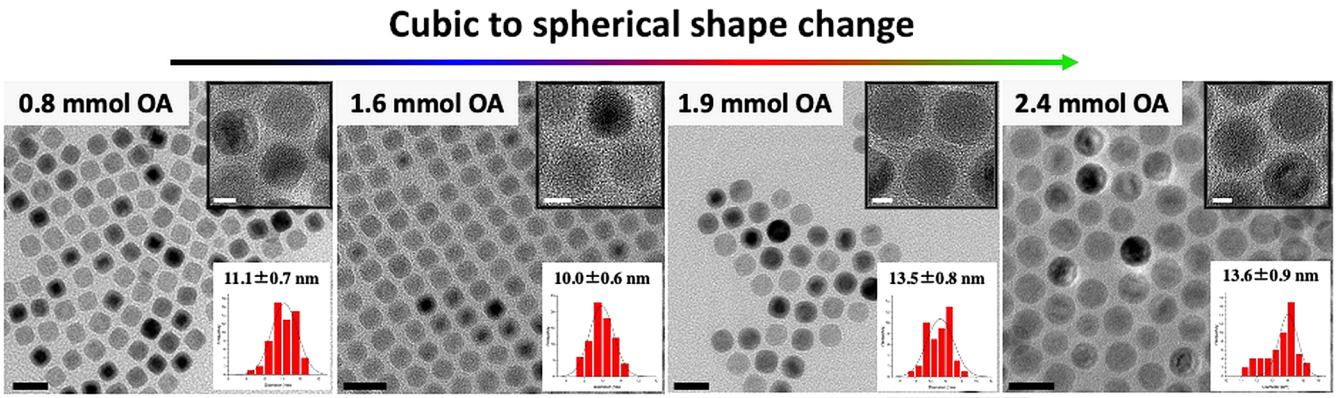

Figure 1. Size and shape variation of IONCs (scale bars: 20 nm) as a function of the OA amount in the reaction mixture together with zoom-in transmission electron microscopy (TEM) images (scale bar: 5 nm) in the inset.

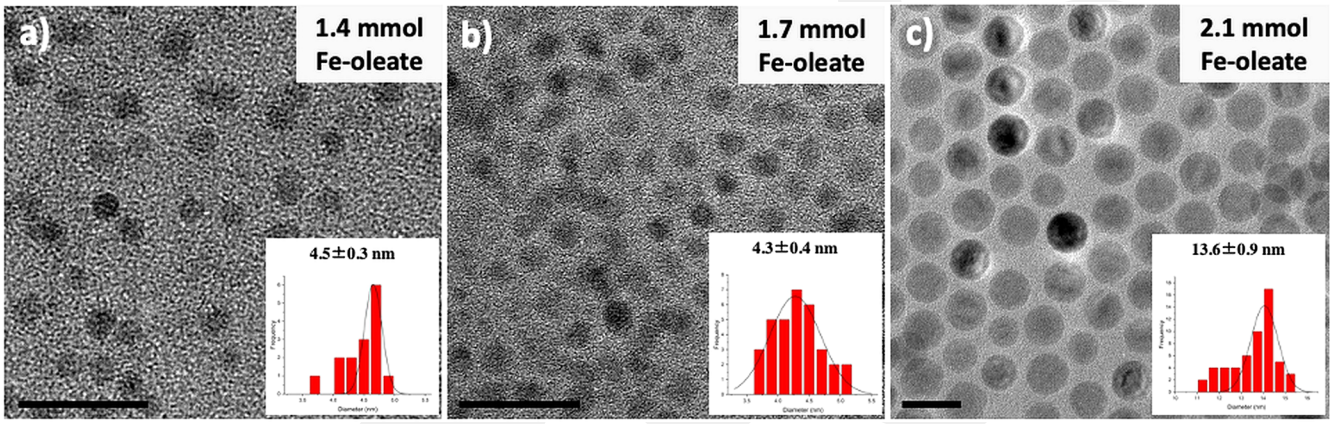

Figure 2. IONCs synthesized with the indicated amounts of Fe-oleate using 2.4 mmol of OA and 25 mL of ODE solution (scale bars: 20 nm).

and electrodeposition) and chemical procedures (co-precipitation, emulsion, hydrolysis of iron salt, and decomposition of the organic iron precursor) have been used to control the shape and the size of the IONCs.[16−19] More recently, Chen et al.[20] fabricated almost-defect-free ferrite nanoparticles by stabilizing the metastable wüstite state by tuning the nonaqueous redox phase.

Few reports in the literature yield IONCs with a well-defined structure, size distribution, shape, and magnetic properties.[21−23] Among them, high-temperature decomposition of iron-oleate is one of the best synthesis approaches to produce large-scale magnetic IONCs exhibiting monodispersity in size and shape together with control on the crystal structure.[18,24,25] Depending on the reaction conditions, different sizes, shapes, and crystal structures can be obtained by this method. To enable the formation of cubic IONCs, using an additional sodium-oleate (Na-oleate) complex is a well-known and the most preferred approach in most synthesis protocols reported to date.[11,26] Although numerous papers are published on the iron-oleate-based thermal decomposition synthesis of IONCs,[21,23] there is insufficient understanding of how to simultaneously control the nanoparticle size and shape while keeping the particle size distribution within the required limits for the formation of nanoparticle mesocrystals.

In this work, the parameters determining the sphere or cube nanoparticle formation and the size of IONCs are studied in detail. After the morphological and magnetic characterization of these IONCs, we demonstrated and discussed the evaporation-driven magnetic field-induced assembly of nanocubes into highly ordered cuboid mesocrystals. We believe that the insights gained from this study will have significant implications on the future development of nanocrystals as building blocks to form large-scale mesocrystals.

RESULTS AND DISCUSSION

By exploiting the high-temperature decomposition of the Fe-oleate method, the growth of IONCs in varying sizes and shapes was systematically studied by altering synthesis parameters (oleic acid, Fe-oleate, and the heating rate). Here, we first investigated the size and the shape effect of oleic acid (OA) on IONCs, a widely preferred organic molecule as a stabilizer in the synthesis of different nanocrystals, including IONCs,[16,18] and colloidal semiconductor quantum dots.[27] We varied the OA concentration in the reaction mixture while keeping other parameters fixed to understand its effect on the size and the morphology of IONCs (Figure 1). In all of these syntheses, we set the amount of Fe-oleate to be 2.1 mmol, ODE to be 25 mL, and the heating temperature to be 5.5 °C/min (Table S1 in the Supporting Information (SI)). Figure 1 reveals that the increased OA amount favors the shape change from cubic to spherical. Since the OA is a fatty acid with relatively long chains, it strongly coordinates the ligand in the IONC synthesis and promotes preferable ligand bonding to specific facets. Castellanos-Rubio et al.[19] reported that using higher amounts of OA induces spherical particle formation instead of anisotropic octahedral particles due to increased steric hindrance, which correlates with our results. An excess amount of OA may also surround

https://doi.org/10.1021/acsomega.1c02322
ACS Omega 2021, 6, 20351−20360

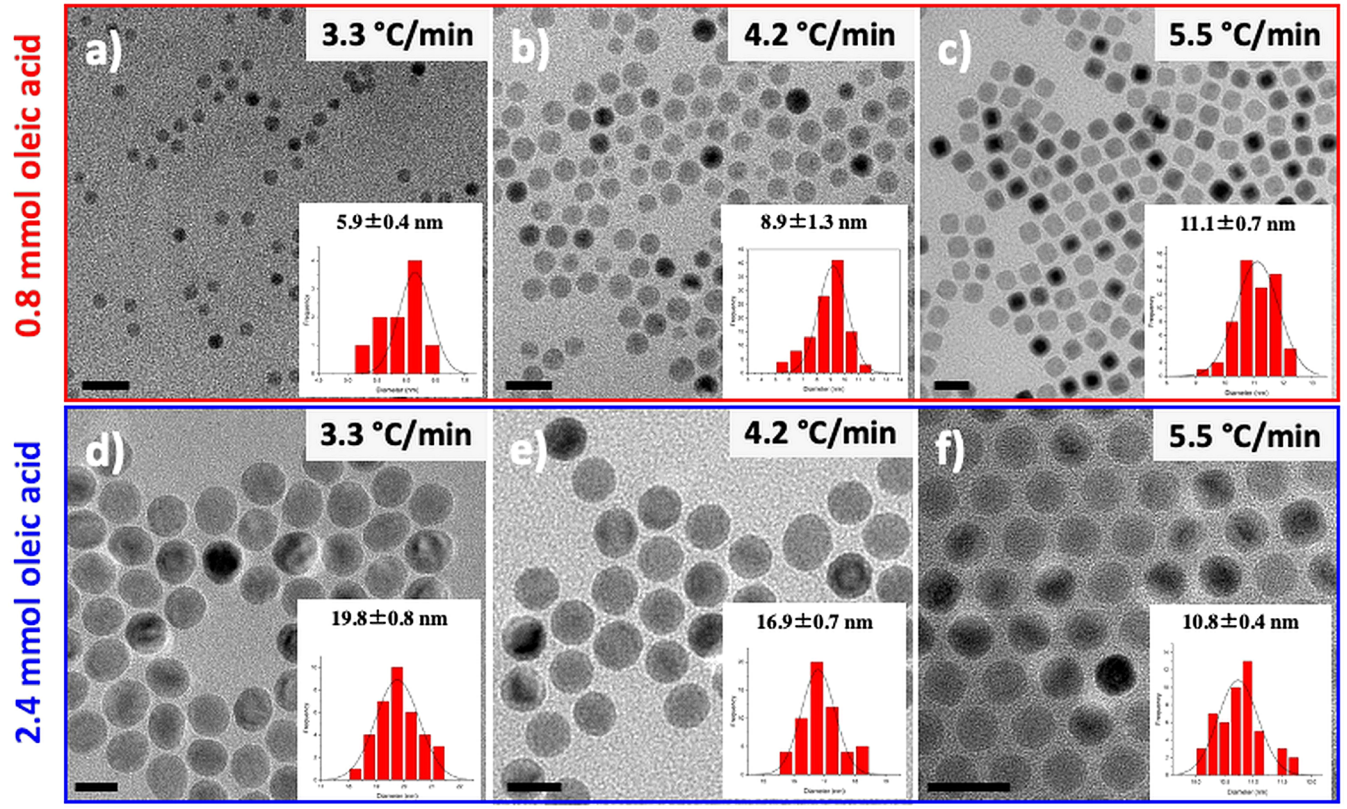

Figure 3. Influence of the heating rate on the morphological change of IONCs synthesized in the presence of 2.1 mmol of Fe-oleate and 0.8 and 2.4 mmol of OA, separately (scale bars: 20 nm).

the nanocrystals more homogenously during nucleation and slow down the particle growth rate, which results in the formation of smoother and rounder IONCs.

When we compare the sizes of IONCs in Figure 1, we observe a slight increase in the size (from ~11.0 to 13.5 nm) with increasing OA concentration, as also reported in other studies.[28,29] The relation between Ostwald ripening and the length of the fatty acid caused this trend. Briefly, depending on the ligand concentration, the monodisperse NCs obtained before the Ostwald ripening stage have a fixed size when fatty acids having relatively long chains such as OA and stearic acid were used.[30] Higher concentrations of OA can decrease the nucleation process by redissolving the as-formed small nuclei and allow for only the large nuclei to grow. This process results in larger nanoparticles with the increase of OA concentrations. Although the OA concentration increases in the synthesis mixture, the relation between the added OA and the OA per nanoparticle was unclear. To understand this relation, OA per nanoparticle is calculated for 0.8 and 2.4 mmol of the added groups and found to be 7.22 and 13.56 × 10^{-21} mol, respectively. This result shows that the OA concentration used in the synthesis is correlated with the attached OA per nanoparticle, but it is not directly proportional to it. The details of the calculations are provided in the SI.

The iron-oleate (Fe-oleate) concentration is also known to affect the IONC size and shape.[25,31,32] Since our previous results show that OA concentrations of 2.4 and 0.8 mmol strongly affect the nanoparticle size and shape, we also evaluated the effect of varying the Fe-oleate concentration in 2.4 mmol of OA, including groups. TEM images of these syntheses are presented in Figure 2, and the detailed synthesis parameters are given in Table S2 in the SI. Results demonstrated that increasing concentrations of Fe-oleate form larger IONCs with improved homogenous size distribution, whereas they do not affect the shape (spherical for all Fe-oleate concentrations) (Figure 2). This suggests that the OA concentration is the main parameter affecting the shape. Moreover, there is a critical concentration of Fe-oleate, which affects the size of the NCs. Lower amounts of Fe-oleate form very small nuclei but do not allow for these nanocrystals to grow enough, leading to the formation of particle sizes smaller than 5 nm (Figure 2a,b). However, when its concentration was increased to 2.1 mmol, larger and smoother spherical IONCs were obtained. Most likely, this occurs due to the decreased nucleation because of the increased concentration of decomposed Fe-oleate monomers.[14]

In the syntheses with a high OA concentration discussed above (2.4 mmol), there is a vital amount of Fe-oleate for a homogenous size distribution of IONCs synthesized, which is found to be 2.1 mmol in our study (Figure 2c). Therefore, instead of using lower concentrations of Fe-oleate (1.4 and 1.7 mmol), we synthesized IONCs using 2.1 and 2.4 mmol of Fe-oleate for the 0.8 mmol of OA-added syntheses (Figure S1 and Table S2 in the SI). Results confirm that 0.8 mmol of OA supports the formation of cubic NCs. Also, it is observed that increased Fe-oleate (from 2.1 to 2.4 mmol) triggers an increase in the size from 11.0 ± 0.7 to 12.9 ± 1.8 nm in the cubic IONCs similar to the spherical ones. Interestingly, particle size distribution increased when we used 2.4 mmol of Fe-oleate. The thermal decomposition of Fe-oleate is rapid at high temperatures. We believe this broadening is due to the excess amount of Fe-oleate (Fe-oleate/OA ratio is 3), which forms

https://doi.org/10.1021/acsomega.1c02322
ACS Omega 2021, 6, 20351−20360

Table 1. Optimized Synthesis Parameters for Highly Monodisperse Similar-Sized Cubic and Spherical IONCs along with Their Sizes

IONCs	size (nm)	Fe-oleate (mmol)	oleic acid (mmol)	ODE (mL)	heating rate (°C/min)
cube	10.8 ± 0.8 (edge-to-edge)	2.1	0.8	25	5.5
sphere	11.3 ± 0.5 (diameter)	2.1	2.4	25	5.3

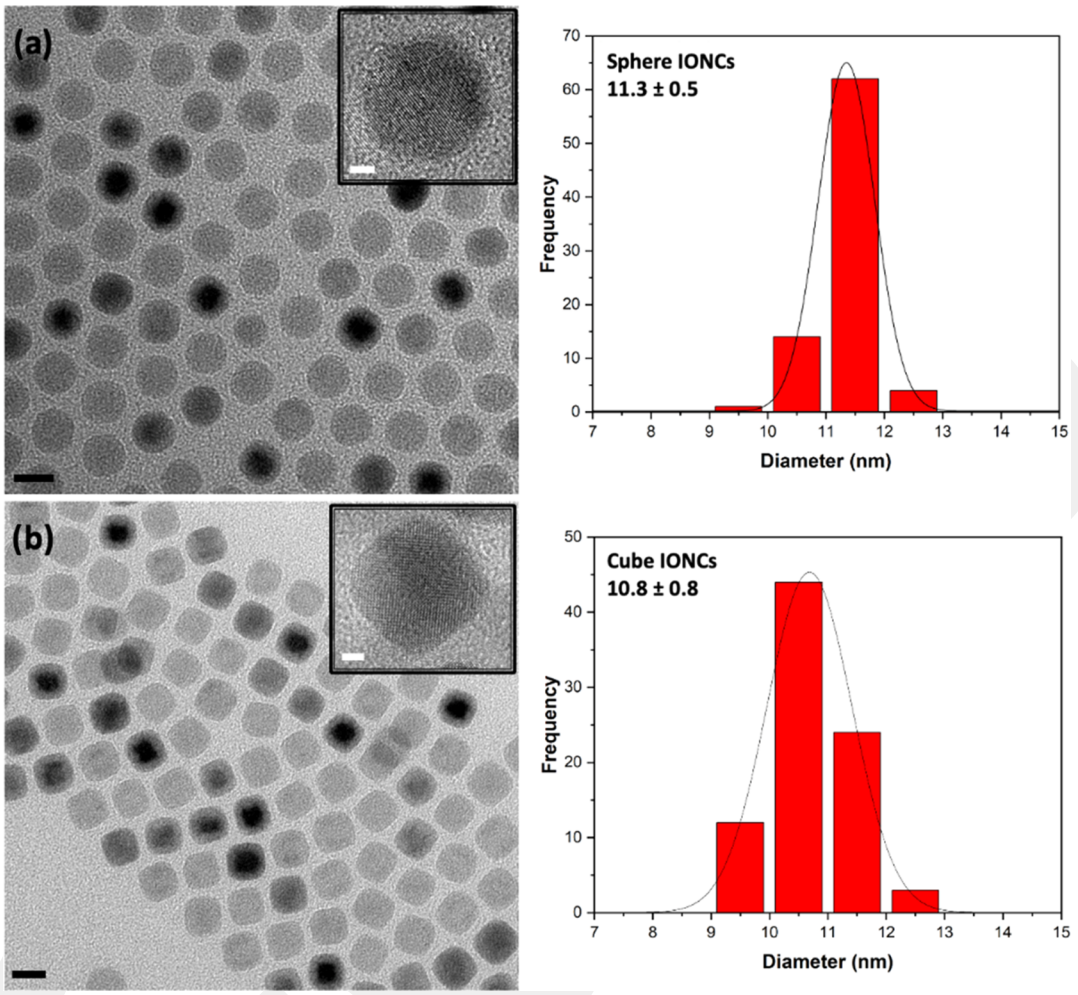

Figure 4. TEM images and Gaussian-fitted size distribution histograms of (a) spherical IONCs and (b) cubic IONCs (scale bars: 10 nm). The insets show the zoomed-in images of a single particle (scale bars: 2 nm).

high concentrations of monomers. Supersaturation of these monomers either induce second nucleation or redistribution of monomers between particles during the ripening process.[14]

We also investigated the effect of the heating rates (3.3, 4.2, and 5.5 °C/min) on the size and shape of IONCs synthesized when the OA concentration was 0.8 and 2.4 mmol while keeping the Fe-oleate concentration at 2.1 mmol (Table S3). As shown in Figure 3a−c, in the 0.8 mmol of OA-added syntheses, average sizes of the IONCs were measured to be 5.9 ± 0.4, 8.9 ± 1.3, and 11.0 ± 0.7 nm when they are synthesized at a constant heating rate of 3.3, 4.2, and 5.5 °C/min, respectively. This increase in the size was accompanied by a shape change from sphere to cube with an increasing heating rate. On the other hand, when the OA concentration increases to 2.4 mmol, only spherical IONCs are obtained. The average sizes of these spherical IONCs are measured to be 19.8 ± 0.8, 16.9 ± 0.7, and 10.8 ± 0.4 nm with the same increasing heating rates, respectively, in line with the previous reports on spherical IONCs.[19,33]

Our results clearly indicate that both OA concentration and the heating rate contribute to the final shape and size of the nanoparticles. When the heating rate is low, OA molecules most likely have more time to be homogeneously dispersed on the nanoparticles, which results in the formation of spherical IONCs. As the heating rate increases, the nucleation process increases, and competition between the nucleation process and the surface passivation of OA molecules takes place. At lower OA concentrations, this competition seems to favor the formation of cubes with increasing sizes as the heating rate increases. At higher OA concentrations, the increasing heating rates cause nucleation to be stronger. However, the OA concentration is now high enough to stabilize a larger number of smaller IONCs while maintaining the spherical shape. Therefore, a reduction in the particle size is observed as the heating rate increases at high OA concentrations. These results show that the heating rate does not affect the shape of the IONCs if the OA concentration is higher than a critical value. Considering the report of Ahniyaz et al.,[10] where only spherical

https://doi.org/10.1021/acsomega.1c02322
ACS Omega 2021, 6, 20351−20360

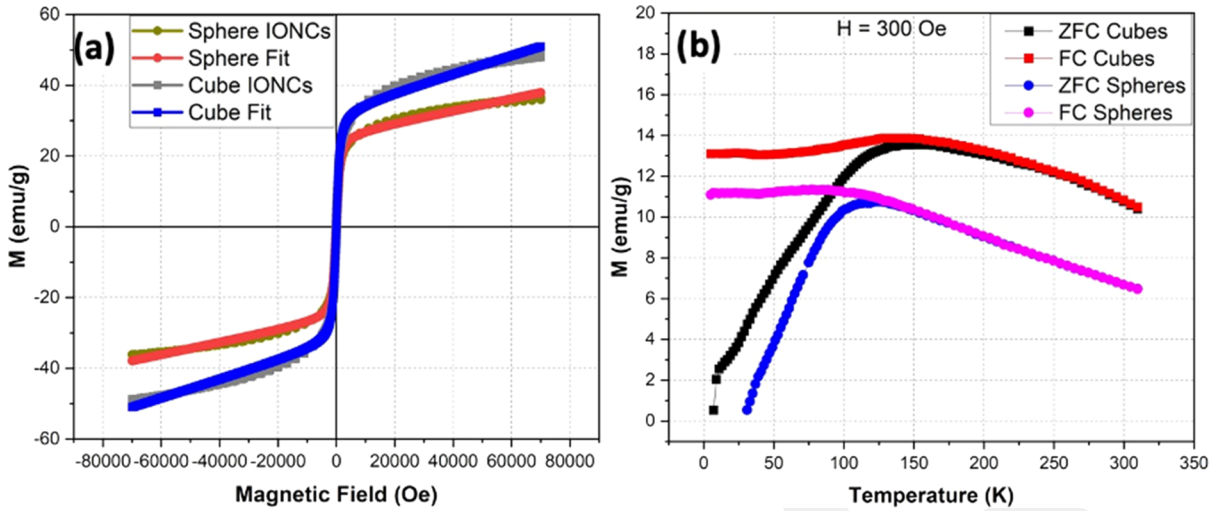

Figure 5. (a) M−H curves and their corresponding fits obtained using eq 1 for ∼11 nm sized IONCs and (b) zero field- (ZFC) and field-cooled (FC) M−T curves of the same IONCs.

IONCs are obtained at heating rates above 3 °C/min at an iron-oleate/oleic acid molar ratio of 3.5 (3.0 in our case), we conclude that only spherical IONCs are obtained if the heating rate and the OA concentration are both high enough. At low OA concentrations, the interplay between nucleation and particle stabilization by OA causes the formation of larger cubic IONCs at increased heating rates. Nevertheless, the physical mechanisms behind these observations are not yet fully understood, and further studies are needed to explain them.

It is understood that nanocrystals having remarkably similar sizes can crystallize into the desired mesocrystals.[1,3,34] Therefore, following the detailed investigation on the size- and the shape-affecting parameters, we tailored the synthesis of precisely controlled and highly monodisperse cubic and spherical IONCs having approximately similar sizes (∼11.0 nm) and examined their structural and magnetic properties. The optimized parameters used to synthesize highly monodisperse ∼11 nm sized cubic (edge-to-edge length) and spherical (diameter) IONCs are summarized in Table 1, and TEM images of these IONCs with their respective size distribution histograms are presented in Figure 4. As depicted in Figure 4, the particle size distribution is narrow for both nanospheres and nanocubes, with an average size of 11.3 ± 0.5 and 10.8 ± 0.8 nm, respectively.

We also observed that our nanocubes appear slightly truncated. To determine the degree of truncation, we followed an approach similar to that of Disch et al.[35] Briefly, the average truncation length ($t_i = (t_{ia} + t_{ib})/2$) and each of the cube edges (l_i) were determined manually from the TEM images, and the truncation parameter (τ_i) was calculated using $\tau_i = 2t_i/l_i$. Since this measurement is suitable for [100] zone axis-oriented nanocubes, we measured more cubelike particles in the TEM images. Results demonstrated that the mean value of the truncation degree for our nanocubes was $\tau = 0.43$ with a standard deviation of $\sigma_\tau = 0.23$, which is closer to the ideal cube ($\tau = 0$) than a cuboctahedron ($\tau = 1$) (Figure S3 in the SI). We also compared the OA percentage of nanospheres and nanocubes using thermogravimetric analysis (TGA). Results revealed that the OA percentages in the ∼11 nm sized nanocubes and nanospheres are 22.6 and 39.1 wt %, respectively (Figure S4 in the SI).

We subsequently studied the magnetic properties of these cubic and spherical IONCs having an ∼11 nm edge-to-edge size using a vibrational sample magnetometer to measure magnetization dependence on the magnetic field (M−H curve) and temperature (M−T curve). We recorded M−H curves at body temperature (310 K) because of their potential use as a contrast agent in clinical MRI, and the experimental data and the corresponding fits for spherical and cubic IONCs are presented in Figure 5a.

Here, we see a continuous growth of magnetization along with the magnetic field, which suggests that these IONCs may have a partially paramagnetic (PM) behavior in addition to their superparamagnetic (SPM) nature. To test this hypothesis, these mixed magnetic phases were investigated by fitting the M−H curves of the samples using eq 1

$$M(T) = M_s\left[\coth\left(\frac{m_p H}{k_B T}\right) - \left(\frac{k_B T}{m_p H}\right)\right] + \chi_a H \quad (1)$$

where $M(T)$ represents the magnetization of the nanocrystals at temperature T, M_s denotes the saturation magnetization of the nanocrystals, m_p is the average magnetic moment per particle, χ_a is the linear component of susceptibility, and k_B is the Boltzmann constant.[36] The SPM and PM contributions to the total magnetic moment can be observed in the first and second terms of eq 1, respectively. The fitting parameters obtained for ∼11 nm sized nanospheres and nanocubes using eq 1 are presented in Table 2. As observed in both Figure 5 and Table 2, our experimental data and the SPM + PM fit matched well, substantiating the presence of both SPM and PM phases. This PM property in IONCs may stem from the enhanced spin canting of IONCs.[16] Additionally, we found

Table 2. Fitting Parameters Obtained for 11 nm Sized IONCs Using eq 1[a]

IONCs	M_s (emu/g)	χ_a (emu/g·Oe)	m_p (μ_B)	H_c (Oe)	T_B (K)
cube	33.12	2.58×10^{-4}	9890	111	135
sphere	26.21	1.69×10^{-4}	10 025	120	120

[a]The table also presents the coercive field (H_c) and blocking temperature (T_B) for these IONCs.

https://doi.org/10.1021/acsomega.1c02322
ACS Omega 2021, 6, 20351−20360

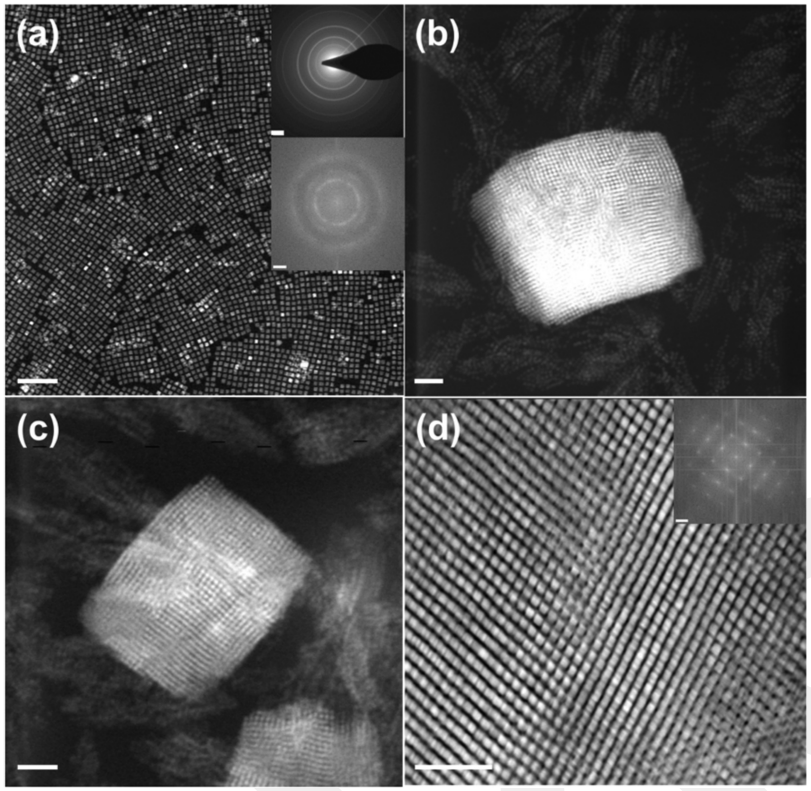

Figure 6. TEM images of the nanocubes (a) in the absence of a magnetic field (H = 0 mT) along with its SAED pattern (upper inset, scale bar: 2 1/nm) and FFT image (lower inset, scale bar: 50 1/μm). (b, c). Cuboid mesocrystals obtained from the nanocubes with a concentration of 15 wt % in hexane under a 180 mT magnetic field (d) High-magnification images of the cuboid mesocrystals along with its FFT image as shown in the inset (scale bars for all TEM images: 100 nm, for FFT image: 50 1/μm).

that the saturation magnetization (M_s) values for cubic and spherical IONCs were 33.12 and 26.21 emu/g, respectively.

Similar to our results, Zhen et al.[28] reported higher M_s values for 8 nm sized cubical IONCs (~40 emu/g) in comparison to similar-sized spherical NCs (~31 emu/g). In another study, similar comparative results were reported by Luigjes et al.,[37] where it was argued that superior magnetic properties were expected from the cubic IONCs rather than the spherical ones. Facets in cubic IONCs suggest that particle growth is sufficiently slow for the preferential development of energetically favored surface crystal planes. In contrast, sphericity suggests that particle growth is very fast, which results in a high concentration of crystal defects and poor magnetic properties. On the contrary, Li et al.[38] reported roughly similar magnetization saturation values for comparable sizes of spherical (12 nm; $M_s \sim$ 48.7 emu/g) and cubic (11.3 nm; $M_s \sim$ 45.3 emu/g) nanocrystals. These different reports emerge since the magnetic properties of the IONCs are both anisotropy and size-dependent.

We also observed that the linear component of susceptibility (χ_a) has a larger value (2.58×10^{-4} emu/g·Oe) for the nanocubes in comparison to the nanospheres (1.69×10^{-4} emu/g·Oe), which indicates a stronger paramagnetic component for nanocubes (Table 2). This implies that the r_1 relaxivity values for the nanocubes should be higher than their spherical counterparts, which supports the reports in the literature.[28,31,39] We also found that coercivity (H_c) in our study is not zero above the blocking temperature (T_B), which is expected for a purely superparamagnetic sample. From the M−T curves, we obtain the blocking temperature (T_B) values for cubic and spherical IONCs to be 135 and 120 K, respectively (Figure 5b). These observations further strengthen our claim that our IONCs possess a paramagnetic (PM) component in addition to their superparamagnetic (SPM) component.

Finally, we studied the formation of ordered nanocrystal arrays and mesocrystals of these highly monodisperse cubic IONCs in the presence of a magnetic field. It is known that IONCs can be formed in different phases depending on their oxidation states, and these structural differences have a critical effect on magnetic properties.[20] To understand the crystal structure of as-synthesized cubic IONCs that are used in mesocrystal formation, we performed XRD measurements. From the XRD data (Figure S5 in the SI), it is found that the XRD peaks lie between the magnetite and maghemite structure but closer to the maghemite structure, as shown in Table S4 in the SI. Within the resolution of XRD measurements, we did not observe the presence of the FeO phase in the XRD pattern. Afterward, superlattices were obtained by solution evaporation (overnight drying) of IONCs (15 wt % in hexane) on a TEM grid at RT in the presence of a 180 mT magnetic field inside a vial. Although hexane evaporates within a short period (in our case, the evaporation was slow because the vial cap was closed during the experiment), there are still trace amounts of other low-volatile compounds such as ODE and OA in the nanocrystal dispersion, which provides the necessary fluidity for the wet particle monolayer to induce particle rearrangement into a densely packed configuration.[40] The magnetic-field-induced dipole−dipole interaction between the individual nanocubes and the van der Waals attraction forces are responsible for the slow growth of large, highly ordered 3D superlattices.[9,10] Therefore, it is possible to create highly

https://doi.org/10.1021/acsomega.1c02322
ACS Omega 2021, 6, 20351−20360

ordered defect-free mesocrystals under a relatively weak magnetic field.[10] However, there are contradictory studies on this subject in the literature. For instance, Rosenfeldt et al.[41] claim that the formation of 3D structures is not induced by the evaporation of the solvent, which is not observed in our study. This report is also quite contradictory to the earlier reports stating that mesocrystals are formed by solvent evaporation within a magnetic field.[10,42]

In this work, we also tested the use of spherical IONCs, lower concentrations of cubic IONCs (5 wt %), and the effect of the magnetic field on the formation of superlattices. The experiments performed with the ∼11 nm sized spherical IONCs demonstrated that there is no superlattice assembly with or without a magnetic field (data not shown), as also reported in the literature.[9] Similarly, we did not observe any mesocrystal formation without the application of a magnetic field on cubic IONCs, as depicted in Figure 6a. The selected area electron diffraction (SAED) pattern shown in the upper inset of Figure 6a suggests that the IONCs distribute randomly in the absence of a magnetic field. The fast Fourier transform (FFT) image shown in the lower inset of Figure 6a also confirmed the random orientation of nanocubes in the absence of a magnetic field. Recently, Kapuscinski et al.[43] reported a two-stage assembly of mesocrystal fibers in the presence of a weak magnetic field. In the first stage, cuboid mesocrystals are formed by the evaporation-driven assembly in the absence of a magnetic field. In the second stage, the cuboid mesocrystals align and attach in an oriented fashion along the magnetic field to form mesocrystal fibers. Additionally, Rosenfeldt et al.[41] claimed that 3D cuboids can be formed at high concentrations of NCs even without the application of a magnetic field, which is also confirmed by the studies of Wetterskog et al.[25] and Agthe et al.[44] However, in our case, we did not observe any cuboid mesocrystals even at high concentrations (15 wt %) in the absence of a magnetic field. Then, we applied a magnetic field to a high concentration of cubic IONCs, and we observed highly ordered ∼300−500 nm sized cuboid superstructures (Figure 6b,c). We have also obtained TEM images of cuboid mesocrystals at different magnifications, which are presented in Figure S6 in the SI. These cuboid mesocrystals maintained a constant separation of ∼3.2 nm, as visible from Figure 6d. We believe that the low-volatile nature of ODE and OA governed this distance during the drying process, and it corresponds to the thickness of the interdigitated OA coating layer on the nanocube surfaces. The line profile of Figure 6d is presented in Figure S7 in the SI, which also supports this claim. This has been further substantiated by the presence of 22.6 wt % OA in the nanocubes from the TGA results. Also, as presented in the inset of Figure 6d, the FFT pattern of these thick 3D mesocrystals suggests that they have a high degree of orientational order in the presence of the magnetic field. There may be some defects in these mesocrystals, which can be minimized using smoother substrates instead of the TEM grids that we used in this study. Since the significance of nanoparticle solution concentration in the 3D superlattice formation is known in the literature, we also investigated 5 wt % IONCs under a magnetic field (in hexane). Although Rosenfeldt et al.[41] found that a magnetic field is needed for the formation of 3D cuboids using cubic IONCs (8.2 nm) at low temperatures and low concentrations, we did not observe any 3D cuboid structure when we used a low concentration of IONCs and even when a magnetic field was applied (data not shown).

CONCLUSIONS

Here, we systematically studied the synthesis conditions to produce highly monodisperse nanocubes suitable for assembling large, ordered arrays. First, we investigated the effect of oleic acid, iron-oleate, and the heating rate on the synthesis of IONCs in the desired shape and size. Morphological analyses demonstrated that the oleic acid concentration is mainly responsible for the shape change and the Fe-oleate amount in the reaction is critical for size variation. Afterward, we synthesized monodisperse ∼11 nm cubic and spherical IONCs as a building block in mesocrystal formation for mesocrystal experiments. Magnetic characterizations of both cubic and spherical IONCs revealed a paramagnetic phase in addition to their superparamagnetic phase. We have demonstrated the formation of the assembly of nanocubes in the presence of a magnetic field and observed cuboid mesocrystal formations at high concentrations (i.e., 15 wt %). In contrast, the spherical IONCs, a lower concentration (5 wt %) of cubic IONCs, and the absence of a magnetic field do not lead to 3D mesocrystals. Mesocrystals with a high degree of crystallographic orientational order obtained in this study may have application in various fields, such as optoelectronics, energy storage, and biomedicine.

EXPERIMENTAL DETAILS

Materials. Oleic acid (OA), 1-octadecene (ODE), and iron(III) chloride hexahydrate were purchased from Sigma-Aldrich. Sodium hydroxide, ethanol, hexane, 2-propanol, and other reagents were purchased from Merck.

Synthesis of IONCs. For the synthesis of IONCs, we used a modified procedure reported previously.[14,18] Sodium-oleate (Na-oleate) and iron-oleate (Fe-oleate) are synthesized as described in ref 16. In a typical procedure, 25 mL of ODE solution containing OA and freshly synthesized Fe-oleate was stirred and degassed under vacuum at 70 °C for 2 h. Subsequently, the reaction temperature was increased to 320 °C at a mentioned constant heating rate under an argon flow and kept at this temperature for 30 min to allow for nanocrystal growth. Syntheses of cubic IONCs were performed without the addition of Na-oleate or other chemicals different from the literature.[18,24] To understand the effect of OA and Fe-oleate on the size and the shape change, varying amounts of these chemicals (0.8, 1.6, 1.9, and 2.4 mmol of OA; 1.4, 1.7, and 2.1 mmol of Fe-oleate) were used (Tables S1 and S2). We also investigated the effect of the heating rate (3.3, 4.2, and 5.5 °C/min) on the size and shape of IONCs (Table S3). After the growth of nanocrystals, the solution was cooled to room temperature. For cleaning, 2-propanol was added to the synthesis solution, and the nanocrystals were precipitated at 4500 rpm for 20 min by centrifugation. After removing the supernatant, the samples were washed with acetone three times. IONCs were then dispersed in hexane and filtered using a 0.2 μm Millipore filter. In all experiments, OA-capped IONCs were used.

Structural and Magnetic Characterizations of IONCs. The effects of various parameters (e.g., OA, Fe-oleate, and the rate of temperature increase) on the size and shape were investigated using transmission electron microscopy (TEM) (Tecnai G2 F30). The sizes of the IONCs were calculated from TEM images using ImageJ software. The PEBBLES software[45] was used to calculate the log-normal size distributions of the nanocrystals, and the data were fitted to

https://doi.org/10.1021/acsomega.1c02322
ACS Omega 2021, 6, 20351−20360

a Gaussian function. The crystal structure of the ∼11 nm cubic IONCs was studied using an X-ray diffractometer (XRD) employing Cu Kα (1.54 Å) radiation. Thermal gravimetric analysis (TGA) was performed using a thermogravimetric analyzer Q500 (TA Instruments) to understand the percentage ratio of OA and iron oxide. TGA was carried out between 30 and 600 °C with a heating rate of 20 °C/min. Magnetic properties (M−H and M−T) of IONCs were measured using a vibrating sample magnetometer (Quantum Design PPMS 6000).

Mesocrystals Assembly and Characterization. We prepared cubic and spherical IONCs with concentrations of 5 and 15 wt % in hexane and dipped a TEM grid into these dispersions in a vial. Two magnets facing each other are placed at equal distance from the vial (vial at the center). The strength of the magnetic field was controlled by varying the distance between the magnets and was measured with a Gaussmeter. The variation of the magnetic field with the distance between the two magnets is shown in Figure S8 in the SI. In our case, the distance between the magnets was fixed at 1.7 cm resulting in a magnetic field equivalent to 180 mT. Then, the solvents were allowed to evaporate overnight (15 h) with and without the magnetic field.

■ ASSOCIATED CONTENT

Supporting Information

The Supporting Information is available free of charge at https://pubs.acs.org/doi/10.1021/acsomega.1c02322.

TEM images of IONCs synthesized with varying amounts of Fe-oleate; syntheses parameters and sizes of IONCs represented in Figures 1−3; calculation of the number of the OA molecules per nanoparticle; truncation parameter analysis of cube IONCs; TGA curves of cubic and spherical IONCs; XRD pattern of IONCs; TEM images of cuboid mesocrystals at different magnifications; line profile of Figure 6d; and variation of the magnetic field intensity with the distance between the two magnets (PDF)

■ AUTHOR INFORMATION

Corresponding Author

Hilmi Volkan Demir − *LUMINOUS! Center of Excellence for Semiconductor Lighting and Displays, School of Electrical and Electronic Engineering, School of Physical and Mathematical Sciences, Nanyang Technological University, Singapore 639798, Singapore; UNAM-National Nanotechnology Research Center and Institute of Materials Science and Nanotechnology, Department of Electrical and Electronics Engineering, Department of Physics, Bilkent University, Ankara 06800, Turkey;* orcid.org/0000-0003-1793-112X; Email: hvdemir@ntu.edu.sg

Authors

Zeliha Soran-Erdem − *Department of Engineering Sciences, Abdullah Gul University, Kayseri 38080, Turkey; UNAM-National Nanotechnology Research Center and Institute of Materials Science and Nanotechnology, Department of Electrical and Electronics Engineering, Department of Physics, Bilkent University, Ankara 06800, Turkey*

Vijay Kumar Sharma − *LUMINOUS! Center of Excellence for Semiconductor Lighting and Displays, School of Electrical and Electronic Engineering, School of Physical and Mathematical Sciences, Nanyang Technological University, Singapore 639798, Singapore; UNAM-National Nanotechnology Research Center and Institute of Materials Science and Nanotechnology, Department of Electrical and Electronics Engineering, Department of Physics, Bilkent University, Ankara 06800, Turkey;* orcid.org/0000-0002-2028-5715

Pedro Ludwig Hernandez-Martinez − *LUMINOUS! Center of Excellence for Semiconductor Lighting and Displays, School of Electrical and Electronic Engineering, School of Physical and Mathematical Sciences, Nanyang Technological University, Singapore 639798, Singapore; UNAM-National Nanotechnology Research Center and Institute of Materials Science and Nanotechnology, Department of Electrical and Electronics Engineering, Department of Physics, Bilkent University, Ankara 06800, Turkey;* orcid.org/0000-0001-6158-0430

Complete contact information is available at: https://pubs.acs.org/10.1021/acsomega.1c02322

Author Contributions

Z.S.-E. and V.K.S. contributed equally to this work. The manuscript was written through the contributions of all authors. All authors have given approval to the final version of the manuscript.

Notes

The authors declare no competing financial interest.

■ ACKNOWLEDGMENTS

The authors acknowledge the financial support from TUBITAK (115F297, 117E713, and 119N343). H.V.D. gratefully acknowledges support from TÜBA.

■ REFERENCES

(1) Sturm née Rosseeva, E. V.; Cölfen, H. Mesocrystals: Structural and Morphogenetic Aspects. *Chem. Soc. Rev.* **2016**, *45*, 5821−5833.

(2) Zhou, L.; O'Brien, P. Mesocrystals — Properties and Applications. *J. Phys. Chem. Lett.* **2012**, *3*, 620−628.

(3) Ma, M.-G.; Cölfen, H. Mesocrystals — Applications and Potential. *Curr. Opin. Colloid Interface Sci.* **2014**, *19*, 56−65.

(4) Wu, W.; Wu, Z.; Yu, T.; Jiang, C.; Kim, W.-S. Recent Progress on Magnetic Iron Oxide Nanoparticles: Synthesis, Surface Functional Strategies and Biomedical Applications. *Sci. Technol. Adv. Mater.* **2015**, *16*, No. 023501.

(5) Disch, S.; Wetterskog, E.; Hermann, R. P.; Korolkov, D.; Busch, P.; Boesecke, P.; Lyon, O.; Vainio, U.; Salazar-Alvarez, G.; Bergström, L.; et al. Structural Diversity in Iron Oxide Nanoparticle Assemblies as Directed by Particle Morphology and Orientation. *Nanoscale* **2013**, *5*, 3969.

(6) Lv, Z.-P.; Kapuscinski, M.; Bergström, L. Tunable Assembly of Truncated Nanocubes by Evaporation-Driven Poor-Solvent Enrichment. *Nat. Commun.* **2019**, *10*, No. 4228.

(7) Brunner, J.; Baburin, I. A.; Sturm, S.; Kvashnina, K.; Rossberg, A.; Pietsch, T.; Andreev, S.; Sturm née Rosseeva, E.; Cölfen, H. Self-Assembled Magnetite Mesocrystalline Films: Toward Structural Evolution from 2D to 3D Superlattices. *Adv. Mater. Interfaces* **2017**, *4*, No. 1600431.

(8) Brunner, J. J.; Krumova, M.; Cölfen, H.; Sturm née Rosseeva, E. V. Magnetic Field-Assisted Assembly of Iron Oxide Mesocrystals: A Matter of Nanoparticle Shape and Magnetic Anisotropy. *Beilstein J. Nanotechnol.* **2019**, *10*, 894−900.

(9) Mehdizadeh Taheri, S.; Michaelis, M.; Friedrich, T.; Förster, B.; Drechsler, M.; Römer, F. M.; Bösecke, P.; Narayanan, T.; Weber, B.; Rehberg, I.; et al. Self-Assembly of Smallest Magnetic Particles. *Proc. Natl. Acad. Sci. U.S.A.* **2015**, *112*, 14484−14489.

(10) Ahniyaz, A.; Sakamoto, Y.; Bergstrom, L. Magnetic Field-Induced Assembly of Oriented Superlattices from Maghemite Nanocubes. *Proc. Natl. Acad. Sci. U.S.A.* **2007**, *104*, 17570−17574.
(11) Singh, G.; Chan, H.; Baskin, A.; Gelman, E.; Repnin, N.; Kral, P.; Klajn, R. Self-Assembly of Magnetite Nanocubes into Helical Superstructures. *Science* **2014**, *345*, 1149−1153.
(12) Singh, G.; Chan, H.; Udayabhaskararao, T.; Gelman, E.; Peddis, D.; Baskin, A.; Leitus, G.; Král, P.; Klajn, R. Magnetic Field-Induced Self-Assembly of Iron Oxide Nanocubes. *Faraday Discuss.* **2015**, *181*, 403−421.
(13) Jiang, C.; Leung, C. W.; Pong, P. W. T. Magnetic-Field-Assisted Assembly of Anisotropic Superstructures by Iron Oxide Nanoparticles and Their Enhanced Magnetism. *Nanoscale Res. Lett.* **2016**, *11*, No. 189.
(14) Jiang, F.; Li, X.; Zhu, Y.; Tang, Z. Synthesis and Magnetic Characterizations of Uniform Iron Oxide Nanoparticles. *Phys. B: Condens. Matter* **2014**, *443*, 1−5.
(15) Liang, X.; Wang, X.; Zhuang, J.; Chen, Y.; Wang, D.; Li, Y. Synthesis of Nearly Monodisperse Iron Oxide and Oxyhydroxide Nanocrystals. *Adv. Funct. Mater.* **2006**, *16*, 1805−1813.
(16) Sharma, V. K.; Alipour, A.; Soran-Erdem, Z.; Aykut, Z. G.; Demir, H. V. Highly Monodisperse Low-Magnetization Magnetite Nanocubes as Simultaneous T 1 − T 2 MRI Contrast Agents. *Nanoscale* **2015**, *7*, 10519−10526.
(17) Sayed, F. N.; Polshettiwar, V. Facile and Sustainable Synthesis of Shaped Iron Oxide Nanoparticles: Effect of Iron Precursor Salts on the Shapes of Iron Oxides. *Sci. Rep.* **2015**, *5*, No. 9733.
(18) Park, J.; An, K.; Hwang, Y.; Park, J.-G.; Noh, H.-J.; Kim, J.-Y.; Park, J.-H.; Hwang, N.-M.; Hyeon, T. Ultra-Large-Scale Syntheses of Monodisperse Nanocrystals. *Nat. Mater.* **2004**, *3*, 891−895.
(19) Castellanos-Rubio, I.; Rodrigo, I.; Munshi, R.; Arriortua, O.; Garitaonandia, J. S.; Martinez-Amesti, A.; Plazaola, F.; Orue, I.; Pralle, A.; Insausti, M. Outstanding Heat Loss via Nano-Octahedra above 20 Nm in Size: From Wustite-Rich Nanoparticles to Magnetite Single-Crystals. *Nanoscale* **2019**, *11*, 16635−16649.
(20) Chen, R.; Christiansen, M. G.; Sourakov, A.; Mohr, A.; Matsumoto, Y.; Okada, S.; Jasanoff, A.; Anikeeva, P. High-Performance Ferrite Nanoparticles through Nonaqueous Redox Phase Tuning. *Nano Lett.* **2016**, *16*, 1345−1351.
(21) Laurent, S.; Forge, D.; Port, M.; Roch, A.; Robic, C.; Vander Elst, L.; Muller, R. N. Magnetic Iron Oxide Nanoparticles: Synthesis, Stabilization, Vectorization, Physicochemical Characterizations, and Biological Applications. *Chem. Rev.* **2008**, *108*, 2064−2110.
(22) Jeong, U.; Teng, X.; Wang, Y.; Yang, H.; Xia, Y. Superparamagnetic Colloids: Controlled Synthesis and Niche Applications. *Adv. Mater.* **2007**, *19*, 33−60.
(23) Kwon, S. G.; Hyeon, T. Colloidal Chemical Synthesis and Formation Kinetics of Uniformly Sized Nanocrystals of Metals, Oxides, and Chalcogenides. *Acc. Chem. Res.* **2008**, *41*, 1696−1709.
(24) Sun, S.-N.; Wei, C.; Zhu, Z.-Z.; Hou, Y.-L.; Venkatraman, S. S.; Xu, Z.-C. Magnetic Iron Oxide Nanoparticles: Synthesis and Surface Coating Techniques for Biomedical Applications. *Chin. Phys. B* **2014**, *23*, No. 037503.
(25) Wetterskog, E.; Agthe, M.; Mayence, A.; Grins, J.; Wang, D.; Rana, S.; Ahniyaz, A.; Salazar-Alvarez, G.; Bergström, L. Precise Control over Shape and Size of Iron Oxide Nanocrystals Suitable for Assembly into Ordered Particle Arrays. *Sci. Technol. Adv. Mater.* **2014**, *15*, No. 055010.
(26) Kovalenko, M. V.; Bodnarchuk, M. I.; Lechner, R. T.; Hesser, G.; Schäffler, F.; Heiss, W. Fatty Acid Salts as Stabilizers in Size- and Shape-Controlled Nanocrystal Synthesis: The Case of Inverse Spinel Iron Oxide. *J. Am. Chem. Soc.* **2007**, *129*, 6352−6353.
(27) Erdem, T.; Soran-Erdem, Z.; Sharma, V. K.; Kelestemur, Y.; Adam, M.; Gaponik, N.; Demir, H. V. Stable and Efficient Colour Enrichment Powders of Nonpolar Nanocrystals in LiCl. *Nanoscale* **2015**, *7*, 17611−17616.
(28) Zhen, G.; Muir, B. W.; Moffat, B. A.; Harbour, P.; Murray, K. S.; Moubaraki, B.; Suzuki, K.; Madsen, I.; Agron-Olshina, N.; Waddington, L.; et al. Comparative Study of the Magnetic Behavior of Spherical and Cubic Superparamagnetic Iron Oxide Nanoparticles. *J. Phys. Chem. C* **2011**, *115*, 327−334.
(29) Klomp, S.; Walker, C.; Christiansen, M.; Newbold, B.; Griner, D.; Cai, Y.; Minson, P.; Farrer, J.; Smith, S.; Campbell, B. J.; et al. Size-Dependent Crystalline and Magnetic Properties of 5−100 Nm Fe_3O_4 Nanoparticles: Superparamagnetism, Verwey Transition, and FeO−Fe_3O_4 Core−Shell Formation. *IEEE Trans. Magn.* **2020**, *56*, 1−9.
(30) Jana, N. R.; Chen, Y.; Peng, X. Size- and Shape-Controlled Magnetic (Cr, Mn, Fe, Co, Ni) Oxide Nanocrystals via a Simple and General Approach. *Chem. Mater.* **2004**, *16*, 3931−3935.
(31) Zhou, Z.; Zhu, X.; Wu, D.; Chen, Q.; Huang, D.; Sun, C.; Xin, J.; Ni, K.; Gao, J. Anisotropic Shaped Iron Oxide Nanostructures: Controlled Synthesis and Proton Relaxation Shortening Effects. *Chem. Mater.* **2015**, *27*, 3505−3515.
(32) Bronstein, L. M.; Huang, X.; Retrum, J.; Schmucker, A.; Pink, M.; Stein, B. D.; Dragnea, B. Influence of Iron Oleate Complex Structure on Iron Oxide Nanoparticle Formation. *Chem. Mater.* **2007**, *19*, 3624−3632.
(33) Stepanov, A.; Mendes, R.; Rümmeli, M.; Gemming, T.; Nizameev, I.; Mustafina, A. Synthesis of Spherical Iron-Oxide Nanoparticles of Various Sizes under Different Synthetic Conditions. *Chem. Pap.* **2019**, *73*, 2715−2722.
(34) Josten, E.; Angst, M.; Glavic, A.; Zakalek, P.; Rücker, U.; Seeck, O. H.; Kovács, A.; Wetterskog, E.; Kentzinger, E.; Dunin-Borkowski, R. E.; et al. Strong Size Selectivity in the Self-Assembly of Rounded Nanocubes into 3D Mesocrystals. *Nanoscale Horiz.* **2020**, *5*, 1065−1072.
(35) Disch, S.; Wetterskog, E.; Hermann, R. P.; Salazar-Alvarez, G.; Busch, P.; Brückel, T.; Bergström, L.; Kamali, S. Shape Induced Symmetry in Self-Assembled Mesocrystals of Iron Oxide Nanocubes. *Nano Lett.* **2011**, *11*, 1651−1656.
(36) Pisane, K. L.; Despeaux, E. C.; Seehra, M. S. Magnetic Relaxation and Correlating Effective Magnetic Moment with Particle Size Distribution in Maghemite Nanoparticles. *J. Magn. Magn. Mater.* **2015**, *384*, 148−154.
(37) Luigjes, B.; Woudenberg, S. M. C.; de Groot, R.; Meeldijk, J. D.; Torres Galvis, H. M.; de Jong, K. P.; Philipse, A. P.; Erné, B. H. Diverging Geometric and Magnetic Size Distributions of Iron Oxide Nanocrystals. *J. Phys. Chem. C* **2011**, *115*, 14598−14605.
(38) Li, W.; Lee, S. S.; Wu, J.; Hinton, C. H.; Fortner, J. D. Shape and Size Controlled Synthesis of Uniform Iron Oxide Nanocrystals through New Non-Hydrolytic Routes. *Nanotechnology* **2016**, *27*, No. 324002.
(39) Alipour, A.; Soran-Erdem, Z.; Utkur, M.; Sharma, V. K.; Algin, O.; Saritas, E. U.; Demir, H. V. A New Class of Cubic SPIONs as a Dual-Mode T1 and T2 Contrast Agent for MRI. *Magn. Reson. Imaging* **2018**, *49*, 16−24.
(40) Rabani, E.; Reichman, D. R.; Geissler, P. L.; Brus, L. E. Drying-Mediated Self-Assembly of Nanoparticles. *Nature* **2003**, *426*, 271−274.
(41) Rosenfeldt, S.; Förster, S.; Friedrich, T.; Rehberg, I.; Weber, B. Self-Assembly of Magnetic Iron Oxide Nanoparticles Into Cuboidal Superstructures. In *Novel Magnetic Nanostructures*; Domracheva, N.; Caporali, M.; Rentschler, E. B. T.-N. M. N., Eds.; Elsevier, 2018; pp 165−189.
(42) Josten, E.; Wetterskog, E.; Glavic, A.; Boesecke, P.; Feoktystov, A.; Brauweiler-Reuters, E.; Rücker, U.; Salazar-Alvarez, G.; Brückel, T.; Bergström, L. Superlattice Growth and Rearrangement during Evaporation-Induced Nanoparticle Self-Assembly. *Sci. Rep.* **2017**, *7*, No. 2802.
(43) Kapuscinski, M.; Munier, P.; Segad, M.; Bergström, L. Two-Stage Assembly of Mesocrystal Fibers with Tunable Diameters in Weak Magnetic Fields. *Nano Lett.* **2020**, *20*, 7359−7366.
(44) Agthe, M.; Wetterskog, E.; Mouzon, J.; Salazar-Alvarez, G.; Bergström, L. Dynamic Growth Modes of Ordered Arrays and Mesocrystals during Drop-Casting of Iron Oxide Nanocubes. *CrystEngComm* **2014**, *16*, 1443−1450.

https://doi.org/10.1021/acsomega.1c02322
ACS Omega 2021, 6, 20351−20360

(45) Mondini, S.; Ferretti, A. M.; Puglisi, A.; Ponti, A. Pebbles and PebbleJuggler: Software for Accurate, Unbiased, and Fast Measurement and Analysis of Nanoparticle Morphology from Transmission Electron Microscopy (TEM) Micrographs. *Nanoscale* **2012**, *4*, 5356.

https://doi.org/10.1021/acsomega.1c02322
ACS Omega 2021, 6, 20351−20360